Effects of Mass Ablation on the Scaling of X-Ray Power with Current in Wire-Array *Z* Pinches

R. W. Lemke, D. B. Sinars, E. M. Waisman, M. E. Cuneo, E. P. Yu, T. A. Haill, H. L. Hanshaw, T. A. Brunner, C. A. Jennings, W. A. Stygar, M. P. Desjarlais, T. A. Mehlhorn, and J. L. Porter

Sandia National Laboratories, P.O. Box 5800, Albuquerque, New Mexico 87185, USA

(Received 8 August 2008; published 15 January 2009)

X-ray production by imploding wire-array *Z* pinches is studied using radiation magnetohydrodynamics simulation. It is found that the density distribution created by ablating wire material influences both x-ray power production, and how the peak power scales with applied current. For a given array there is an optimum ablation rate that maximizes the peak x-ray power, and produces the strongest scaling of peak power with peak current. This work is consistent with trends in wire-array *Z* pinch x-ray power scaling experiments on the *Z* accelerator.

DOI: 10.1103/PhysRevLett.102.025005 PACS numbers: 52.59.Qy

Z pinch implosions using cylindrical wire arrays composed of hundreds of tungsten wires are an effective means of producing intense bursts (~100–220 TW) of soft x-rays [1–4] (0.1–10 keV). On the *Z* accelerator, Joule heating turns the ~10 μm diameter wires into plasma in the first few ns (nanoseconds) of the applied current (peak ~20 MA). The magnetic force ($J \times B$) on the current carrying plasma implodes it to the z axis on a time scale of ~100 ns where some of its energy is thermalized and radiated in a burst of x-ray power several ns in duration. The wire-array *Z* pinch is a promising x-ray source for indirect drive, inertial confinement fusion (ICF) concepts. In one approach, x-rays from two *Z* pinches irradiate a hohlraum containing a nuclear fuel capsule. Computational studies of this target design require a three-stage x-ray drive pulse with a peak power ~1000 TW to achieve a fusion yield of ~500 MJ [5]. Experiments on *Z* have shown that wire-array *Z* pinches can produce the required x-ray pulse shape [6], but the required current drive (~100 ns rise time, ~60 MA peak current) is beyond present capabilities. Consequently, it is of great interest to understand how the x-ray power (P_R) produced by a wire-array *Z* pinch scales with applied current (I_{load}). It has been argued that P_R should scale like I_{load}^2 because the pinch kinetic energy scales similarly. However, initial experiments by Stygar *et al.* [2] on *Z* using 300 wire, 1 cm length (L) and radius (R), tungsten arrays produced $P_R \propto I_{\mathrm{load}}^{1.24\pm0.18}$, for 2.7 and 5.9 mg arrays that imploded in ~95 ns (τ_{imp}). Later experiments by Mazarakis *et al.* [7] with 1.1 and 2.5 mg arrays yielded $P_R \propto I_{\mathrm{load}}^{1.71\pm0.10}$, for load currents of 11.2 and 17.0 MA, and $\tau_{\mathrm{imp}} = 80$ ns. It is important to understand the cause of subquadratic scaling in these experiments in order to assess the feasibility of wire-array *Z* pinches for high current ICF.

In this Letter we present results of a computational study of x-ray power production by tungsten wire arrays that reveal an explanation for the trends observed in these current scaling experiments, and that provide insight on the physics that influence how P_R varies with I_{load}. Experiments performed on *Z* using single arrays [2–4,7] with masses in the range $1.15 \le M \le 30.0$ mg are modeled using 2D (two-dimensional) RMHD (radiation magnetohydrodynamic) simulations. We find that the density distribution created by ablating wire material significantly affects the scaling of P_R with I_{load}, and for a given array mass there is an optimum ablation rate that maximizes P_R.

This numerical study was performed using the 3D, RMHD code ALEGRA [8]. The computational domain is a 3D wedge in cylindrical polar coordinates ($r\theta z$), $0 \le z \le L = 1$ cm, $0 \le r \le 1.5$–1.6 cm, $R = 1$ cm, $0 \le \theta \le 1°$, with cell sizes $\Delta z = \Delta r = 50$ μm, and $\Delta\theta = 1°$. With only one cell in θ the geometry is azimuthally symmetric (i.e., 2D). Physics models include resistive MHD coupled to an equivalent circuit representation of the *Z* accelerator [9], Ohm's law $\vec{J} = \sigma(\vec{E} + \vec{v} \times \vec{B})$, single group radiation diffusion for $M \le 6$ mg, implicit Monte Carlo radiation otherwise, thermal conduction, separate electron and ion temperatures, equations of state, electrical and thermal conductivities, tabular opacities, and artificial viscosity (Q). Shock heating of material occurs through Q, and is consistent with the jump conditions for shocks. In these Eulerian simulations, a Lagrangian step is followed by a remap to the original mesh.

In lieu of modeling individual wires in the array, a mass injection scheme is used to emulate material ablating from the wires [10–14]. There is ample experimental evidence in support of a long-lived ablation phase that determines the dynamics of the final implosion to the axis [3,10,15]. The mass ablation rate per zone, per unit length, at the array radius (R), as a function of the time dependent magnetic field [$B(t)$] is

$$\frac{dm}{dt} = \dot{M}_0 \left[\frac{B(t)}{B_n}\right]^{1.4} [1 + \varepsilon p(z)] \left(\frac{\Delta z \Delta\theta}{2\pi L}\right), \qquad (1)$$

where $B_n = 300$ T; $\dot{M}_0$ (kg/m s) depends on the array mass through the wire diameter; the exponent 1.4 is obtained in a steady state theory of ablation [12]. Mass is injected with radial velocity $v_0 = -2 \times 10^4$ m/s, and a

prescribed density perturbation [$\varepsilon p(z)$], until the total array mass (M) is injected. The injected mass forms a conducting ablation plasma that is swept at high velocity (~100–150 km/s) by the magnetic field toward the axis [Fig. 1(a)]. The function $\varepsilon p(z)$, plotted in Fig. 1(b), is an axially nonuniform perturbation with a normal distribution of wavelengths about 300 μm. It produces the short wavelength, nonuniform, axial ablation [Fig. 1(c)] observed in experiments [10], which evolves into a longer wavelength magnetic Rayleigh Taylor (MRT) instability [4,6,10,15] as the pinch implodes [Fig. 1(d)].

This 2D simulation model produces some features of 3D simulations [13,14] that influence the x-ray pulse, including trailing mass and current. A consequence of 2D azimuthal symmetry is that current does not flow in θ, so a greater fraction of the current flows in a smaller fraction of the mass than in 3D, which results in a narrower x-ray pulse. We mitigate this effect for a given mass by averaging x-ray powers (and related quantities) from 3–5 simulations with different phases of $\varepsilon p(z)$.

The perturbation amplitude [ε in Eq. (1)] and $\dot{M}_0(M)$ were determined by simulating a series of experiments [4] on Z in which M was varied by changing the wire diameter (D_w), keeping the wire number (N) fixed at 300. Array masses of 1.15, 2.5, and 6.0 mg were used. For each mass $\dot{M}_0$ and ε were varied [for fixed $p(z)$] until the timing, amplitude, and shapes of the measured and simulated x-ray power $P_R(t)$ and load current $I_{\text{load}}(t)$ were in good agreement; $P_R(t)$ is calculated by integrating the radiation flux over the radial boundary. Simulated and measured $P_R(t)$ are compared in Fig. 2(a). The resulting mass ablation scaling, $\dot{M}_0 \propto M^{0.25} \propto D_w^{0.50}$, is used to adjust Eq. (1) when M is changed. The determined value of $\varepsilon = 1.0$ is fixed in all simulations.

The mechanisms that contribute to the simulated x-ray power are elucidated by the equation $P'_R = P^*_S + P_{\text{PdV}} + P_J - P_I$, which calculates the time dependent x-ray power in terms of sources and sinks of internal energy integrated over the simulation volume; P^*_S, P_{PdV}, and P_J, denote x-ray power produced via shock heating, PdV work, and Joule heating, respectively, and P_I is the power lost to internal energy. An asterisk indicates that energy corrections due to remap losses are included. In shocked regions a numerical loss of kinetic energy can occur during the mesh remap due to the discrete nature of the algorithm, thereby significantly affecting the x-ray power. To mitigate this effect and to conserve energy, the ion internal energy is corrected with an amount equal to that lost. Figure 2(b) plots P^*_S, P_{PdV}, P'_R, and P_R for the 6 mg case shown in Fig. 2(a); the x-ray pulse is dominated by the contribution from shock heating. Internal energy is conserved exactly when $P'_R = P_R$. For array masses up to 30 mg P_R is dominated by P^*_S and P_{PdV}; P_J and P_I can be significant, but typically not until after peak power. Hence, through peak power $J \times B$ work accounts for all energy coupled to the Z pinch plasma which, for the 1.15 mg bare-axis pinch, disagrees with a semi-empirical estimate based on radially resolved emission measurements [4].

The results in Fig. 2(a) are the basis for the simulated current scaling experiments. The implosion times (τ_{imp}) for the 1.15, 2.5, and 6.0 mg arrays are 59.0, 81.1, and 102.3 ns, respectively. Like the experiments [2,7], we determine the scaling of maximum P_R with peak I_{load} for tungsten arrays with the same radius, τ_{imp}, and different M, but similar implosion dynamics. These conditions are satisfied if $I_{\text{load}} \propto M^{0.5}$, and the functional dependence of the current on time is the same [16]. To produce this behavior in simulations, the applied circuit voltage must scale approximately as $M^{0.5}$. Then the normalized waveforms for current and radiated power are nearly identical for arrays with different M and the same τ_{imp}. Similar to the short [7] and

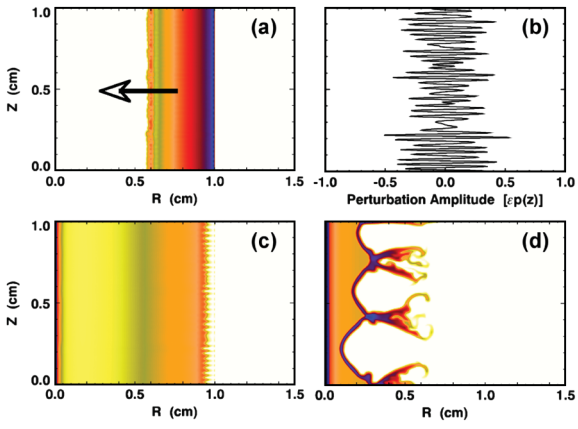

FIG. 1 (color). (a) Density plot of ablated plasma early in time (arrow indicates flow direction). (b) Density perturbation (for $\varepsilon = 0.5$) vs z. (c) Z pinch density at beginning of implosion, and (d) just before stagnation. Dark blue indicates high density.

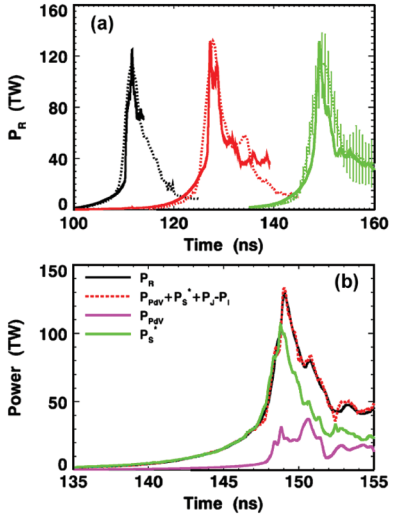

FIG. 2 (color). (a) Measured (dashed) and simulated (solid) x-ray power vs time for arrays with masses 1.15 (black), 2.5 (red), and 6.0 (green) mg (error bars indicate shot-to-shot variation). (b) X-ray power vs time (6 mg array) from shock heating (P^*_S), PdV work (P_{PdV}), all internal energy sources (dashed red), and integrated flux (P_R).

long [2] implosion time experiments, we include 1.15 and 2.5 mg arrays with implosion times of 81.1 and 102.3 ns, respectively. Also included are results for 6.0 and 14.4 mg arrays with implosion times of 81.1 and 102.3 ns, respectively, which were not part of the experiments. The resulting peak x-ray powers (P_R) are plotted versus peak load current ($I_{\rm load}$) in Fig. 3(a). The best fit to each set of simulation points corresponds to $P_R = 0.48 I_{\rm load}^{2.05}$ ($I_{\rm load}$ in MA, P_R in TW) for $\tau_{\rm imp} = 81.1$ ns, and $P_R = 1.85 I_{\rm load}^{1.48}$ for $\tau_{\rm imp} = 102.3$ ns. Similar to the experiments, the scaling of P_R with $I_{\rm load}$ is stronger for arrays with $\tau_{\rm imp} = 81.1$ ns.

Results plotted in Figs. 3(b) and 3(c) provide an explanation for the trend revealed in Fig. 3(a). For a given array mass, the density and velocity of ablated plasma streaming toward the axis depend on the ablation rate [12]. A slow ablation rate produces ablated material with lower density and higher velocity than a fast ablation rate. For long enough ablation time $\tau_{\rm abl}$ (the time at which all wire material is ablated), a shock heated precursor plasma forms on the axis [3,10,14] before the main pinch arrives [Figs. 1(c) and 1(d)]. Figure 3(b) plots the mass in the precursor plasma ($M_{\rm pc}$) versus $I_{\rm load}$ just before the main pinch interacts with it for each case in Fig. 3(a). Increasing $\tau_{\rm imp}$ from 81.1 to 102.3 ns significantly increases the fractional mass in the precursor ($M_{\rm pc}/M$). Also, for the same implosion time $M_{\rm pc}$ increases with increasing $I_{\rm load}$ (or M, since $I_{\rm load} \propto M^{0.5}$). Figure 3(c) plots the ratio $P_S^*/P_{\rm PdV}$ versus $I_{\rm load}$. The reduction in $P_S^*/P_{\rm PdV}$ at the longer implosion time is well correlated with the jump in $M_{\rm pc}$. We conclude that the presence of the precursor plasma on axis weakens the shock interaction that produces x rays during final stagnation, thereby reducing the maximum temperature attainable by the Z pinch plasma via shock heating. Shock interactions weaken further as $M_{\rm pc}$ increases with increasing $I_{\rm load}$, which causes the scaling of P_R with $I_{\rm load}$ to become weaker than quadratic for arrays with $\tau_{\rm imp} = 102.3$ ns. This is an effect of ablation.

Figure 4(a) shows that for a given array there is an ablation rate that maximizes the peak P_R. Figure 4(b) plots the axially averaged, radial density profiles of the pinch plasma for the lowest and highest values of $\dot{M}_0$ in Fig. 4(a), and for the case of maximum P_R, at a time when the main pinch is located at $r \sim 0.85$ cm. The main pinch accretes ablated material as it implodes resulting in different degrees of MRT stabilization [17], similar to gas-puff Z pinches [18]. The lowest (highest) ablation rate provides the most (least) stabilization of the MRT, but results in the largest (smallest) precursor mass. The optimum ablation rate balances these competing effects, producing a radial density profile that provides some snowplow stabilization of the main pinch plasma to MRT while mitigating the deleterious effect of the precursor on x-ray production at stagnation. The possibility that the ablated plasma stabilizes the pinch was first conjectured by Lebedev [10]. Now, because the ablation rate depends on wire number [10,12], an optimum ablation rate implies that there is a corresponding optimum wire number that maximizes P_R. The existence of an optimum wire number has been shown experimentally [19].

Inefficient x-ray power production due to excessive precursor mass is mitigated by reducing $\tau_{\rm abl}$. Integrating Eq. (1) over the entire array assuming $B(t) = \mu_0 \dot{I}_0 t/(2\pi R)$ yields $\tau_{\rm abl} = 1.44(M/\dot{M}_0)^{0.42}(I_n/\dot{I}_0)^{0.58}$, where $I_n = 15$ MA. For fixed M, it is evident that increasing $\dot{I}_0$ or $\dot{M}_0$ (by changing N or using different wire material) reduces $\tau_{\rm abl}$. Alternatively, $\tau_{\rm abl}$ is reduced by decreasing M, or by shaping the current waveform.

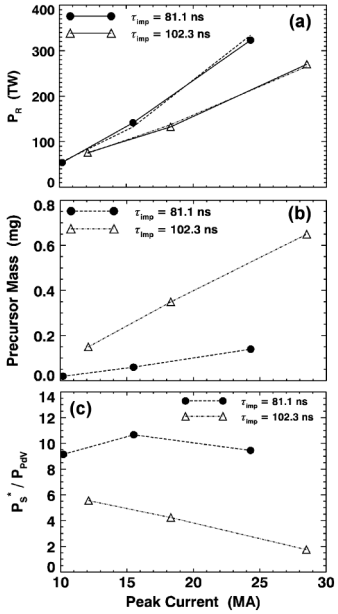

FIG. 3. Peak x-ray power P_R (a), precursor mass $M_{\rm pc}$ (b), and $P_S^*/P_{\rm PdV}$ (c) vs $I_{\rm load}$.

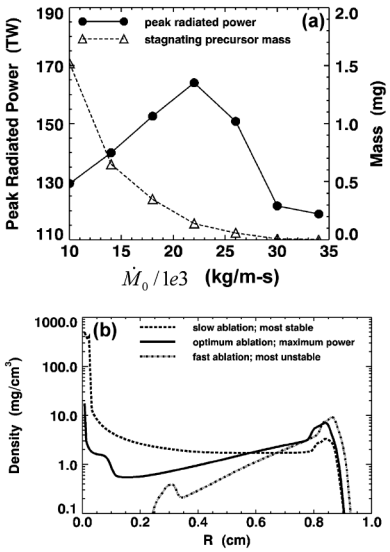

FIG. 4. (a) Peak P_R and $M_{\rm pc}$ vs ablation rate (6 mg array). (b) Axially averaged pinch density at maximum P_R, and at lower and upper bounds in (a).

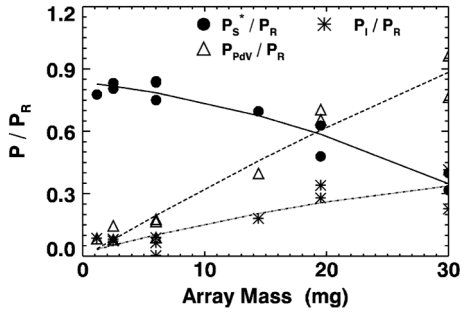

FIG. 5. Fraction of peak x-ray power (P_R) due to shock heating (P_S^*) and PdV work (P_{PdV}), and trapped in internal energy (P_I) vs array mass.

When M is much greater than 6 mg the x-ray power is further affected by the opacity of the Z pinch plasma. Figure 5 plots the ratio of P_S^*, P_{PdV}, and P_I to peak x-ray power P_R versus M for all arrays simulated ($1.15 \leq M \leq 30.0$ mg, $81.1 \leq \tau_{\mathrm{imp}} \leq 221.3$ ns). The 19.5 and 30 mg cases are simulations of experiments on Z. For $M \geq 14.4$ mg the precursor is optically thick (optical depth ≥ 15) due to its large mass ($M_{pc} = 10.0$ mg for $M = 30.0$ mg). Hence, not all of the x-ray energy produced in the stagnating plasma volume is radiated on the time scale of the x-ray pulse, which increases the ratio of internal energy to radiated energy. For $M = 30$ mg an amount of power equal to $\sim$34% of that radiated goes into internal energy at peak x-ray power. It is evident that P_S^* decreases with increasing M, which is well correlated with increasing M_{pc}. Consequently, for $M \geq 19.5$ mg the x-ray power is dominated by heating from PdV work.

A numerical fit to the data for P_R in Fig. 5 yields $P_R = I_{\mathrm{load}}^2/\tau_{\mathrm{therm}}$, for $1.15 \leq M \leq 30.0$ mg, where $\tau_{\mathrm{therm}} = 0.0225\tau_{\mathrm{imp}}(M/2.8)^{0.13}$ is an effective energy thermalization time that accounts for effects of a shock heated precursor, the ablation plasma density profile, and opacity. To compare with experimental scaling we note that [16] $M \propto (I_{\mathrm{load}}\tau_{\mathrm{imp}})^2$, then $\tau_{\mathrm{therm}} \propto I_{\mathrm{load}}^{0.27}\tau_{\mathrm{imp}}^{1.27}$ and $P_R \propto I_{\mathrm{load}}^{1.73}/\tau_{\mathrm{imp}}^{1.27}$. The experimental scaling [20] is $P_R \propto I_{\mathrm{load}}^{1.45\pm0.10}/\tau_{\mathrm{imp}}^{1.34\pm0.17}$, for $1.0 \leq M < 5.9$ mg and $60 \leq \tau_{\mathrm{imp}} \leq 97$ ns, which has the same dependence on τ_{imp} as the simulated scaling. The stronger scaling of the simulated P_R with I_{load} may be due in part to the absence of 3D effects. Nevertheless, the monotonic decrease in P_R with increasing τ_{imp} (and M) agrees with experiment. Since the experimental scaling of P_R with I_{load} is much weaker than quadratic, we conclude that the ablation rate for some (or all) of the arrays used was not optimal for the combination of M and $I_{\mathrm{load}}(t)$.

It has been shown that wire-array Z pinch implosion dynamics are 3D [13,14]. Preliminary results indicate that conclusions based on this 2D model are valid in 3D. Fully 3D simulations of the 2.5 and 6 mg arrays in the mass scan [Fig. 2(a)] produce peak x-ray powers similar to 2D that are dominated by P_S^* (albeit in broader pulses), the dependence of $\dot{M}_0$ on M is similar, and the ratio P_S^*/P_{PdV} is reduced for the larger mass (as in 2D).

The main conclusion of this work is that the rate at which material ablates from wires in an array affects both x-ray power production, and how the peak power scales with applied current. For a given array there is an optimum ablation rate that maximizes the peak x-ray power, and produces the strongest scaling of peak power with peak current. To produce the maximum peak x-ray power for a given current drive it is necessary to optimize both the array mass for maximum kinetic energy generation, and the mass ablation rate of the wires to produce the optimum density profile interior to the main Z pinch plasma. Wire arrays are a feasible x-ray source for ICF if the optimum ablation rate for the required mass [5] is achievable, and if the implosion time can be produced by a current drive that is not precluded by limitations of pulsed power technology.

The authors are grateful to the ALEGRA team at SNL, A. Robinson, W. Rider, S. Petney, E. Love, and R. Summers for their support, and to M. Jones (SNL) for helpful discussions on Z experiments. Sandia is a multiprogram laboratory operated by Sandia Corporation, A Lockheed Martin Company, for the National Nuclear Security Administration under Contract No. DE-AC04-94AL85000.

[1] R. B. Spielman *et al.*, Phys. Plasmas **5**, 2105 (1998); C. Deeney *et al.*, Phys. Rev. Lett. **81**, 4883 (1998).
[2] W. A. Stygar *et al.*, Phys. Rev. E **69**, 046403 (2004).
[3] M. E. Cuneo *et al.*, Phys. Rev. E **71**, 046406 (2005).
[4] D. B. Sinars *et al.*, Phys. Rev. Lett. **100**, 145002 (2008).
[5] J. H. Hammer *et al.*, Phys. Plasmas **6**, 2129 (1999); R. A. Vesey *et al.*, *ibid.* **14**, 056302 (2007).
[6] M. E. Cuneo *et al.*, Phys. Plasmas **13**, 056318 (2006).
[7] M. G. Mazarakis *et al.*, Phys. Rev. E (to be published).
[8] A. C. Robinson *et al.*, Comput. Phys. Commun. **164**, 408 (2004).
[9] R. W. Lemke *et al.*, Phys. Plasmas **10**, 1867 (2003).
[10] S. V. Lebedev *et al.*, Phys. Plasmas **8**, 3734 (2001); Nucl. Fusion **44**, S215 (2004).
[11] V. V. Aleksandrov *et al.*, Plasma Phys. Rep. **27**, 89 (2001); P. V. Sasorov *et al.*, Phys. Plasmas **15**, 022702 (2008).
[12] E. P. Yu *et al.*, Phys. Plasmas **14**, 022705 (2007).
[13] E. P. Yu *et al.*, Phys. Plasmas **15**, 056301 (2008).
[14] J. P. Chittenden *et al.*, Phys. Plasmas **11**, 1118 (2004); Plasma Phys. Controlled Fusion **46**, B457 (2004).
[15] D. B. Sinars *et al.*, Phys. Rev. Lett. **93**, 145002 (2004).
[16] D. D. Ryutov *et al.*, Rev. Mod. Phys. **72**, 167 (2000).
[17] A. L. Velikovich *et al.*, Phys. Rev. Lett. **77**, 853 (1996); J. H. Hammer *et al.*, Phys. Plasmas **3**, 2063 (1996).
[18] H. Sze *et al.*, Phys. Rev. Lett. **95**, 105001 (2005).
[19] M. G. Mazarakis *et al.*, Plasma Devices Oper. **13**, 157 (2005); C. A. Coverdale *et al.*, Phys. Rev. Lett. **88**, 065001 (2002).
[20] M. E. Cuneo, W. A. Stygar, and M. G. Mazarakis (unpublished).